Fetch-limited growth of wind waves

Michael Stiassnie[1]

Received 13 September 2011; revised 8 December 2011; accepted 9 December 2011; published 8 February 2012.

[1] The wave growth mechanisms proposed by Miles (1957) and Phillips (1957) more than 50 years ago, in combination with the concept of the "limiting spectrum," are used to obtain mathematical solutions to the problem of fetch-limited wavefields. Explicit expressions for (1) the spectra, (2) the significant wave height, and (3) the peak frequency in terms of the wind shear velocity and the fetch are given.

Citation: Stiassnie, M. (2012), Fetch-limited growth of wind waves, *J. Geophys. Res.*, *117*, C00J04, doi:10.1029/2011JC007579.

1. Introduction

[2] Fetch-limited growth occurs when a wind of constant magnitude and direction blows perpendicular to a long and straight coastline. The water is assumed deep and the wind blows for a sufficiently long time that the wavefield reaches a steady state. Hence, for a given wind speed, the wavefield becomes a function of the distance from the shoreline, which is termed the fetch.

[3] The case of fetch-limited growth has been extensively investigated both by laboratory and field experiments. Many of the existing results are summarized by *Young* [1999], and in two recent papers by *Hwang* [2006] and *Badulin et al.* [2007]. *Zakharov* [2005] and *Badulin et al.* [2007] relate the experimental findings to analytical results of the weak turbulence theory, based on *Hasselmann*'s [1962] equation.

[4] In this note, we present an alternative theoretical approach, which is based on the combined Miles-Phillips wind input, and the concept of the "limiting spectrum." The problems of (1) air shear flow instability [*Miles*, 1957] and (2) resonance between the surface waves and the air pressure fluctuations [*Phillips*, 1957] are formulated and solved in sections 2 and 3. The Miles and Phillips models appear as a homogeneous solution and a particular solution of the mathematical problem, respectively.

[5] The connection between the deterministic and stochastic formulations, which is needed in order to discuss the spectra of the free surface in terms of the air pressure spectrum, is given in section 4. For the turbulent air pressure spectrum, we build on a recent paper by *Lysak* [2006], whose results are adapted to our needs and presented in section 5.

[6] In section 6, we introduce the concept of the "limiting spectrum," analogous to the concept of "highest wave" for a Stokes wave. This seems to be a convenient way to handle the highly nonlinear energy dissipation due to wave breaking and the weakly nonlinear (but two-dimensional) energy transfer by wave-wave interactions, simultaneously.

[7] The results are presented in section 7, culminating with the following expressions for the significant wave height H_s, and the peak frequency ω_p, in terms of gravity g, air shear velocity u_*, and fetch x:

$$H_s = 0.029\, g^{-0.5} u_* x^{0.5} \tag{1}$$

$$\omega_p = 3.65\, g^{0.75} {u_*}^{-0.5} x^{-0.25} \tag{2}$$

A thorough discussion, including comparison with published theoretical and experimental results, is given in section 8.

2. Formulation

[8] Assuming two-dimensional inviscid and incompressible flows in the water (denoted by subscript w), as well as in the air (denoted by subscript a) above it. Using capital letters for the mean flow, and the notation ($'$, $\sim$) for the (turbulent, wavy) parts of the flow, the following variables are defined: (1) longitudinal air velocity, $U_a(z) + u'_a(x, z, t) + \tilde{u}_a(x, z, t)$; (2) vertical air velocity, $w'_a(x, z, t) + \tilde{w}_a(x, z, t)$; (3) air pressure, $p_o - \rho_a g z + p'_a(x, z, t) + \tilde{p}_a(x, z, t)$, where ρ_a is the density of the air; (4) longitudinal water velocity, $\tilde{u}_w(x, z, t)$; (5) vertical water velocity, $\tilde{w}_w(x, z, t)$; and (6) water pressure, $p_o - \rho_w g z + \tilde{p}_w(x, z, t)$, where ρ_w is the density of water, and p_o is a reference pressure.

[9] U_a is prescribed; and u'_a, w'_a, p'_a are approximated by known result from pipe flows for which $U_a(0) = 0$. The wavy interface between the water and the air is $z = \eta(x, t)$. The continuity equations and the linearized equations of motion, for the wavy flow are:

$$\frac{\partial \tilde{u}_w}{\partial x} + \frac{\partial \tilde{w}_w}{\partial z} = 0 \;\; ; \;\; x \geq 0 \;\; , \;\; z \leq 0 \tag{3a}$$

$$\frac{\partial \tilde{u}_w}{\partial t} = -\frac{1}{\rho_w}\frac{\partial \tilde{p}_w}{\partial x} \;\; ; \;\; x \geq 0 \;\; , \;\; z \leq 0 \tag{3b}$$

$$\frac{\partial \tilde{w}_w}{\partial t} = -\frac{1}{\rho_w}\frac{\partial \tilde{p}_w}{\partial z} \;\; ; \;\; x \geq 0 \;\; , \;\; z \leq 0 \tag{3c}$$

[1]Department of Civil and Environmental Engineering, Technion–Israel Institute of Technology, Haifa, Israel.

0148-0227/12/2011JC007579

$$\frac{\partial \tilde{u}_a}{\partial x}+\frac{\partial \tilde{w}_a}{\partial z}=0 \;\; ; \;\; x\geq 0 \;\; , \;\; z\geq 0 \tag{4a}$$

$$\frac{\partial \tilde{u}_a}{\partial t}+U_a\frac{\partial \tilde{u}_a}{\partial x}+\frac{dU_a}{dz}\tilde{w}_a=-\frac{1}{\rho_a}\frac{\partial \tilde{p}_a}{\partial x} \;\; ; \;\; x\geq 0 \;\; , \;\; z\geq 0 \tag{4b}$$

$$\frac{\partial \tilde{w}_a}{\partial t}+U_a\frac{\partial \tilde{w}_a}{\partial x}=-\frac{1}{\rho_a}\frac{\partial \tilde{p}_a}{\partial z} \;\; ; \;\; x\geq 0 \;\; , \;\; z\geq 0 \tag{4c}$$

[10] The linearized kinematic and dynamic free surface boundary conditions, and the lateral boundary condition are:

$$\tilde{w}_w=\frac{\partial \eta}{\partial t}=\tilde{w}_a \;\; ; \;\; x\geq 0 \;\; , \;\; z=0 \tag{5a}$$

$$\tilde{p}_w-\rho_w g\eta=\tilde{p}_a-\rho_a g\eta+p'_a \;\; ; \;\; x\geq 0 \;\; , \;\; z=0 \tag{5b}$$

$$\eta=0 \;\; ; \;\; x=0 \tag{5c}$$

[11] Note that the small wind induced current in the water, as well as the effects of surface tension have been neglected in this note.

[12] From (5b) it is clear that one can separate the solution of (3a)–(3c) to (5a)–(5c) into two parts, (1) a homogeneous solution (denoted by the subscript M) and (2) a particular solution (denoted by the subscript p), so that

$$(\tilde{u}_w,\tilde{w}_w,\tilde{p}_w,\tilde{u}_a,\tilde{w}_a,\tilde{p}_a,\eta)=\alpha(u_{wM},w_{wM},p_{wM},u_{aM},w_{aM},p_{aM},\eta_M)+ \\ +\left(u_{wp},w_{wp},p_{wp},u_{ap},w_{ap},p_{ap},\eta_p\right) \tag{6}$$

[13] The homogeneous solution satisfies for any x, equations (3a)–(3c), (4a)–(4c), (5a) and

$$p_{wM}-\rho_w g\eta_M=p_{aM}-\rho_a g\eta_M \;\; , \;\; z=0 \tag{7}$$

[14] The particular solution satisfies for any x, equations (3a)–(3c), (4a)–(4c), (5a) and

$$p_{wp}-\rho_w g\eta_p=p_{ap}-\rho_a g\eta_p+p'_a \;\; , \;\; z=0 \tag{8}$$

[15] The constant α in (6) is determined by (5c)

$$\alpha\eta_M+\eta_p=0 \;\; , \;\; x=0 \tag{9}$$

[16] For the particular problem, it is assumed that

$$p'_a=\int_{-\infty}^{\infty}\int_{0}^{\infty}\exp i(\kappa x-\omega t+\varepsilon(\kappa,\omega))\sqrt{2P(\kappa,\omega)d\kappa d\omega} \tag{10}$$

where P is the pressure wave number and frequency power spectrum, and $\varepsilon(\kappa, \omega)$ are random phases.

[17] The discretized presentation of (10) is

$$p'_a=\sum_m\sum_n\Pi_{mn}\exp i(\kappa_m x-\omega_n t) \tag{11a}$$

$$\Pi_{mn}=\sqrt{2P(\kappa_m,\omega_n)\Delta\kappa\Delta\omega}\,e^{i\varepsilon_{mn}}, \tag{11b}$$

$$\varepsilon_{mn}=\varepsilon(\kappa_m,\omega_n) \tag{11c}$$

3. Solution

3.1. The Particular Part

[18] Seeking a solution of the form

$$u_{wp}^{mn}=a_p^{mn}\frac{df_{wp}^{mn}}{dz}\,e^{i(\kappa_m x-\omega_n t)} \tag{12a}$$

$$w_{wp}^{mn}=-i\kappa_m a_p^{mn}f_{wp}^{mn}\,e^{i(\kappa_m x-\omega_n t)} \tag{12b}$$

$$p_{wp}^{mn}=a_p^{mn}\frac{\rho_w}{\kappa_m}\omega_n\frac{df_{wp}^{mn}}{dz}\,e^{i(\kappa_m x-\omega_n t)} \tag{12c}$$

$$u_{ap}^{mn}=a_p^{mn}\frac{df_{ap}^{mn}}{dz}\,e^{i(\kappa_m x-\omega_n t)} \tag{13a}$$

$$w_{ap}^{mn}=-i\kappa_m a_p^{mn}f_{ap}^{mn}\,e^{i(\kappa_m x-\omega_n t)} \tag{13b}$$

$$p_{ap}^{mn}=a_p^{mn}\frac{\rho_a}{\kappa_m}\left\{(\omega_n-\kappa_m U_a)\frac{df_{ap}^{mn}}{dz}+\kappa_m\frac{dU_a}{dz}f_{ap}^{mn}\right\}e^{i(\kappa_m x-\omega_n t)} \tag{13c}$$

[19] Using (3a)–(3c) and (4a)–(4c), one can show that the auxiliary functions f_{wp}^{mn} *and* f_{ap}^{mn} satisfy the equations

$$\frac{d^2f_{wp}^{mn}}{dz^2}-\kappa_m^2 f_{wp}^{mn}=0 \;\; , \;\; z\leq 0 \tag{14}$$

$$\frac{d^2f_{ap}^{mn}}{dz^2}-\left\{\kappa_m^2+\frac{\frac{d^2U_a}{dz^2}}{U_a-\omega_n/\kappa_m}\right\}f_{ap}^{mn}=0 \;\; , \;\; z\geq 0 \tag{15}$$

[20] For the interface

$$\eta_p^{mn}=a_p^{mn}e^{i(\kappa_m x-\omega_n t)} \tag{16}$$

[21] The boundary conditions (5a) and (8) yield

$$f_{wp}^{mn}=f_{ap}^{mn}=\frac{\omega_n}{\kappa_m} \;\; , \;\; z=0 \tag{17a}$$

$$\rho_w(\omega_n^2-g\kappa_m)a_p^{mn}=\rho_a\left\{\omega_n\left(\frac{df_{ap}^{mn}}{dz}+\frac{dU_a}{dz}\right)-g\kappa_m\right\}a_p^{mn} \\ +\kappa_m\Pi_{mn} \;\; , \;\; z=0 \tag{17b}$$

[22] From (17b) one has

$$a_p^{mn} = \frac{\kappa_m \Pi_{mn}}{\rho_w(\omega_n^2 - g\kappa_m) - \rho_a\left\{\omega_n\left(\frac{df_{ap}^{mn}}{dz} + \frac{dU_a}{dz}\right)\Big|_{z=0} - g\kappa_m\right\}} \tag{18}$$

[23] Since $\rho_a \ll \rho_w$, one can in most cases, ignore the second term in the denominator of (18). The exceptions are the cases for which $\omega_n^2 \approx g\kappa_m$.

[24] In principle, the quantity $\left(\frac{df_{ap}^{mn}}{dz}\right)\Big|_{z=0}$ can be obtained from the solution of Rayleigh's equation (15) with the boundary conditions (17a) and a condition at infinity:

$$\frac{df_{ap}^{mn}}{dz} + \kappa_m f_{ap}^{mn} = 0 \quad , \quad z \to \infty \tag{19}$$

3.2. The Homogeneous Part

[25] Seeking a solution of the form

$$u_{wM}^n = \frac{df_{wM}^n}{dz}\, e^{i(k_n x - \omega_n t)}, \tag{20a}$$

$$w_{wM}^n = -ik_n f_{wM}^n e^{i(k_n x - \omega_n t)} \tag{20b}$$

$$p_{wM}^n = \frac{\rho_w}{k_n}\omega_n \frac{df_{wM}^n}{dz}\, e^{i(k_n x - \omega_n t)} \tag{20c}$$

$$u_{aM}^n = \frac{df_{aM}^n}{dz}\, e^{i(k_n x - \omega_n t)}, \tag{21a}$$

$$w_{aM}^n = -ik_n f_{aM}^n\, e^{i(k_n x - \omega_n t)}, \tag{21b}$$

$$p_{aM}^n = \frac{\rho_a}{k_n}\left\{(\omega_n - k_n U_a)\frac{df_{aM}^n}{dz} + k_n \frac{dU_a}{dz} f_{aM}^n\right\} e^{i(k_n x - \omega_n t)} \tag{21c}$$

[26] Using (3a)–(3c) and (4a)–(4c), one can show that the auxiliary functions f_{wM}^n, f_{aM}^n satisfy

$$\frac{d^2 f_{wM}^n}{dz^2} - k_n^2 f_{wM}^n = 0 \quad , \quad z \le 0 \tag{22}$$

$$\frac{d^2 f_{aM}^n}{dz^2} - \left\{k_n^2 + \frac{\frac{d^2 U_a}{dz^2}}{U_a - \omega_n/k_n}\right\} f_{wM}^n = 0 \quad , \quad z \ge 0 \tag{23}$$

[27] For the interface one has

$$\eta_M^n = e^{i(k_n x - \omega_n t)} \tag{24}$$

[28] The boundary conditions (5a) and (7) yield

$$f_{wM}^n = f_{aM}^n = \frac{\omega_n}{k_n} \quad , \quad z = 0 \tag{25}$$

$$\rho_w(\omega_n^2 - gk_n) = \rho_a\left\{\omega_n\left(\frac{df_{aM}^n}{dz} + \frac{dU_a}{dz}\right) - gk_n\right\} \quad , \quad z = 0 \tag{26}$$

[29] One has to solve Rayleigh's equation (23) with boundary conditions (25), (26), and

$$\frac{df_{aM}^n}{dz} + k_n f_{aM}^n = 0 \quad , \quad z \to \infty \tag{27}$$

[30] For the unknown function f_{aM}^n, and the unknown complex wave number k_n.

3.3. The Combined Free Surface

[31] Rewriting (9) in terms of the above solutions

$$\alpha_n \eta_M^n + \sum_m \eta_p^{m\,n} = 0 \quad , \quad x = 0 \tag{28}$$

[32] Substituting (24) and (16) into (28) gives

$$\alpha_n = -\sum_m a_p^{m\,n} \tag{29}$$

[33] The combined free surface is given by

$$\eta = \sum_n \sum_m a_p^{m\,n}\left[e^{i(\kappa_m x - \omega_n t)} - e^{i(k_n x - \omega_n t)}\right] \tag{30}$$

where $a_p^{m\,n}$ is given by (18).

[34] The above result indicates that the homogenous and particular solutions are of similar weight at the vicinity of $x = 0$, as one would expect. However, as it will become clear in section 4, for locations away from $x \approx 0$, the importance of the energy input by the air pressure fluctuations becomes negligible in comparison to that by the shear flow instability process. Nevertheless, the shear flow instability mechanism cannot be started without the initial contribution of the air pressure fluctuations.

3.4. An Approximate Solution

[35] Referring to (18), it is quite clear that unless $(g\kappa_m - \omega_n^2)/\omega_n^2 = O(\rho_a/\rho_w)$, the second term in its denominator is negligible. Otherwise,

$$\left.\frac{df_{ap}^{mn}}{dz}\right|_{z=0} \approx \left.\frac{df_{aM}^n}{dz}\right|_{z=0} \tag{31}$$

[36] Equation (31) results from the fact that when κ_m in (15) is replaced by ω_n^2/g, it becomes the singular counterpart of (23). For a more complete discussion on methods to solve Rayleigh equations, see *Stiassnie et al.* [2006, section 3], in which both the singular and regular approaches are discussed.

[37] Thus, overall, and using (26):

$$a_p^{mn} = \frac{\kappa_m \Pi_{mn}}{\rho_w(\omega_n^2 - g\kappa_m) - \rho_a\left\{\omega_n\left(\frac{df_{aM}^n}{dz} + \frac{dU_a}{dz}\right)\Big|_{z=0} - g\kappa_m\right\}} \approx \frac{\kappa_m \Pi_{mn}}{g\rho_w(k_n - \kappa_m)} \tag{32}$$

[38] Following *Plant* [1982], the approximate solution of (23) is written as:

$$k_n = \frac{\omega_n^2}{g} - 0.08\frac{i\omega_n^4}{g^3}u_*^2 \tag{33}$$

where u_* is the shear velocity.

[39] Note that the ratio between the spatial growth rate, which appears in (33), and the temporal growth rate given by *Plant* [1982], is about 2; for details, see *Stiassnie et al.* [2007].

4. Spectra of the Free Surface

[40] Substituting (32) and (33) into (30), gives

$$\eta = \sum_n \sum_m \frac{\kappa_m \Pi_{mn} e^{i\left(\frac{\omega_n^2}{g}x - \omega_n t\right)}}{g\rho_w\left[\frac{\omega_n^2}{g} - 0.08i\frac{\omega_n^4}{g^3}u_*^2 - \kappa_m\right]}\left\{e^{i\left(\kappa_m - \frac{\omega_n^2}{g}\right)x} - e^{0.08\omega_n^4 u_*^2 x/g^3}\right\} \tag{34}$$

[41] Introducing (11b) into (34) and returning to a continuous presentation:

$$\eta = \int_{-\infty}^{\infty}\int_0^{\infty} e^{i\left(\frac{\omega^2}{g}x - \omega t + \varepsilon(\omega,\kappa)\right)}\frac{\kappa\left\{e^{i\left(\kappa - \frac{\omega^2}{g}\right)x} - e^{\beta x}\right\}}{g\rho_w\left[\frac{\omega^2}{g} - i\beta - \kappa\right]}\sqrt{2P(\kappa,\omega)d\kappa d\omega} \tag{35}$$

where

$$\beta = 0.08\,\omega^4 u_*^2/g^3 \tag{36}$$

[42] Defining s – the frequency spectrum of η as

$$s = \frac{1}{2\pi}\int_{-\infty}^{\infty}\langle\eta(t+\tau)\eta^*(t)\rangle e^{i\omega\tau}d\tau, \tag{37}$$

where the angular brackets denote an ensemble average (taken over the random phases ε).

$$\langle\eta(t+\tau)\eta^*(t)\rangle = 2\int_{-\infty}^{\infty}\int_0^{\infty} e^{-i\tilde{\omega}\tau}\left|\frac{\kappa\left\{e^{i\left(\kappa - \frac{\tilde{\omega}^2}{g}\right)x} - e^{\beta x}\right\}}{g\rho_w\left[\frac{\tilde{\omega}^2}{g} - i\beta - \kappa\right]}\right|^2 \cdot P(\kappa,\tilde{\omega})d\kappa d\tilde{\omega} \tag{38}$$

[43] Substituting (38) into (37) and integrating, first over τ and then over $\tilde{\omega}$ yields:

$$s(\kappa) = 2\int_{-\infty}^{\infty}\left|\frac{\kappa\left[e^{i\left(\kappa - \frac{\omega^2}{g}\right)x} - e^{\beta x}\right]}{g\rho_w\left[\frac{\omega^2}{g} - i\beta - \kappa\right]}\right|^2 P(\kappa,\omega)d\kappa \tag{39}$$

[44] Using the fact that the main contribution to (39) comes from the vicinity of

$$\kappa \approx \frac{\omega^2}{g} \equiv k, \tag{40}$$

[45] Equation (39) is approximated by

$$s(\omega) = \frac{2k^2}{g^2\rho_w^2}P(k,\omega)\int_{-\infty}^{\infty}\frac{\left[1 + e^{2\beta x} - 2e^{\beta x}\cos((\kappa - k)x)\right]d\kappa}{(\kappa - k)^2 + \beta^2} \tag{41}$$

[46] Finally

$$s(\omega) = \frac{2\pi k^2}{g^2\rho_w^2\beta}\left(e^{2\beta x} - 1\right)P(k,\omega) \tag{42}$$

5. Turbulent Pressure Spectrum

[47] A model for the wall pressure spectrum in turbulent pipe flow is given by (31) of *Lysak* [2006]

$$P_3(\kappa,\chi,\omega) \approx 3\rho_a^2\int_0^{\infty}\left(\frac{dU_a}{dz}\right)^2\frac{\vartheta^2}{k_e^5}\frac{\kappa^2\exp\left[-2z\sqrt{\kappa^2+\chi^2}\right]}{\left[1 + (\kappa/k_e)^2 + (\chi/k_e)^2\right]^{17/6}} \cdot \delta(\omega - U_a\kappa)dz \tag{43}$$

where χ is the wave number in the direction perpendicular to the (x, z) plane; ϑ is the root mean square turbulent velocity; and k_e represents the wave number of the energy containing eddies.

[48] For our purposes, one can assume

$$U_a(z) = 2.5u_*\ell n\left(1 + \frac{z}{z_o}\right) \quad , \quad z_o = 0.02\,u_*^2/g \tag{44}$$

[49] Using (47) and (54) in the work by *Lysak* [2006], with the mixing length $L = 0.4z$, gives

$$k_e = 0.75/z, \tag{45a}$$

$$\vartheta(z) = u_* z/\left(z + 0.02\,u_*^2/g\right) \tag{45b}$$

[50] To obtain an estimate for $P(\kappa, \omega)$ of (42), we multiply the integrand of (43) by $2k_e$ and substitute $\chi = 0$ to obtain

$$P(\kappa,\omega) \approx 6\rho_a^2\int_0^{\infty}\left(\frac{dU_a}{dz}\right)^2\frac{\vartheta^2}{k_e^4}\frac{\kappa^2 e^{-2z|\kappa|}}{\left[1 + (\kappa/k_e)^2\right]^{17/6}}\,\delta(\omega - U_a\kappa)dz \tag{46}$$

[51] Changing the variable of integration in (46) from z to U_a, and integrating, gives:

$$P(\kappa,\omega) \approx 6\rho_a^2\left(\frac{dU_a}{dz}\right)\frac{\vartheta^2}{k_e^4}\frac{\kappa e^{-2\kappa z}}{\left[1 + (\kappa/k_e)^2\right]^{17/6}}\Bigg|_{U_a = \omega/\kappa}, \kappa > 0 \tag{47}$$

[52] The fact that $U_a \geq 0$ renders $P(\kappa, \omega) = 0$, for $\kappa < 0$.

[53] For each ω, there is a $z_{cr}(\omega)$, so that

$$U_a(z_{cr}(\omega)) = \omega/k. \tag{48}$$

.

[54] From (47) and (48)

$$P(k,\omega) = 6\rho_a^2 U_a' \frac{\vartheta^2}{k_e^4} \frac{k\, e^{-2kz_{cr}}}{\left[1+(k/k_e)^2\right]^{17/6}} \tag{49}$$

where U_a', k_e, and ϑ are calculated at

$$z_{cr}(\omega) = z_o\{\exp(0.4\omega/k\, u_*) - 1\} \tag{50}$$

6. The Limiting Spectrum

[55] Substituting (49) into (42) yields

$$s(\omega) = \frac{12\pi k^3}{g^2\beta} \cdot \left(\frac{\rho_a}{\rho_w}\right)^2 \cdot \frac{\vartheta^2 U_a'}{k_e^4} \cdot \frac{e^{-2kz_{cr}}}{\left[1+(k/k_e)^2\right]^{17/6}} \cdot \left(e^{2\beta x} - 1\right) \tag{51}$$

[56] Equation (51) can produce unlimited growth, which in reality is hindered by wave breaking and nonlinear interactions. For gravity waves, based on *Hasselmann*'s [1962] theory, there is no option for nonlinear interactions in a unidirectional spectrum, so that wave breaking remains as the main candidate responsible for growth limiting. In the sequel we introduce the concept of the "limiting spectrum," in analogy to the "highest wave" for a Stokes wave.

[57] Assuming a sea surface made of a series of Stokes waves, with well-separated wavelengths

$$\lambda_n = \lambda_o \gamma^n \quad , \quad n = 0, 1, 2, \ldots; \gamma \geq 2 \tag{52}$$

[58] The wave numbers and frequencies of these waves are

$$k_n = \frac{2\pi}{\lambda_o}\, \gamma^{-n}, \tag{53a}$$

$$\omega_n = \sqrt{\frac{2\pi g}{\lambda_o}}\, \gamma^{-n/2} \tag{53b}$$

[59] For the case of a limiting spectrum, all waves are assumed to reach the maximum steepness which causes their breaking $\varepsilon_{\max}$. Thus the amplitudes of these waves and their energies are:

$$a_n = \frac{\lambda_o \varepsilon_{\max}}{2\pi}\, \gamma^n, \tag{54a}$$

$$e_n = \frac{a_n^2}{2} = \frac{\lambda_o^2 \varepsilon_{\max}^2}{8\pi^2}\, \gamma^{2n} \tag{54b}$$

[60] The spacing between the modes, along the frequency axis, for the nth mode is estimated as

$$\Delta\omega_n = \frac{1}{2}(\omega_{n-1} - \omega_{n+1}) = \frac{1}{2}\sqrt{\frac{2\pi g}{\lambda_o}}\gamma^{-n/2}\left(\gamma^{1/2} - \gamma^{-1/2}\right) \tag{55}$$

[61] The spectral value assigned to the n mode can be shown to be:

$$s_n = \frac{e_n}{\Delta\omega_n} = \alpha g^2 \omega_n^{-5}, \tag{56a}$$

$$\alpha = \frac{\gamma^{1/2}\, \varepsilon_{\max}^2}{\gamma - 1} \tag{56b}$$

[62] Since α in (56a) and (56b) is independent of λ_o, one can generalize (56a) and (56b), and write for the limiting spectrum.

$$s_h(\omega) = \alpha\, g^2 \omega^{-5} \tag{57}$$

[63] The coefficient α is evaluated in section 7, based on field experiments. However, it has a theoretical upper bound, given by (56b) with $\gamma = 2$ and $\varepsilon_{\max} = 0.4$, yielding $\alpha_{\max} = 0.23$.

[64] The value $\gamma = 2$ was chosen to provide reasonable separation of length scales, whereas $\varepsilon_{\max} = 0.4$ is based on known results for the highest Stokes wave.

[65] Note that $\alpha = 0.23$ is only an upper bound and that the value which fits experimental evidence is $\alpha = 0.074$, as explained in section 7. Substituting $\gamma = 2$ and $\alpha = 0.074$ in (56b) gives $\varepsilon_{\max} = 0.23$, which is a plausible value for wave breaking. From *Babanin* [2011, p. 267], one can see that for hurricane-like conditions (produced by wind generated by helicopter blades) values higher than $\alpha = 0.05$ were measured.

7. Results

[66] All quantities are made dimensionless, using u^*, g, and ρ_a as a base, and denoted by a tilde. From (49), we get

$$\tilde{P} = \frac{g^2 P}{\rho_a^2 u_*^7} = \frac{6\tilde{U}_a'\tilde{\vartheta}^2\tilde{k}}{\tilde{k}_e} \cdot \frac{e^{-2\tilde{k}\,\tilde{z}_{cr}}}{\left[1+\left(\tilde{k}/\tilde{k}_e\right)^2\right]^{17/6}} \tag{58}$$

where

$$\tilde{\omega} = u_*\omega/g, \tag{59a}$$

$$\tilde{k} = \tilde{\omega}^2 \tag{59b}$$

$$\tilde{z}_{cr} = 0.02\{\exp(0.4/\tilde{\omega}) - 1\} \tag{59c}$$

$$\tilde{U}_a' = 125 \cdot \exp(-0.4/\tilde{\omega}) \tag{59d}$$

$$\tilde{\vartheta} = 0.02\{1 - \exp(-0.4/\tilde{\omega})\} \tag{59e}$$

$$\tilde{k}_e = 0.75/\tilde{z}_{cr} \tag{59f}$$

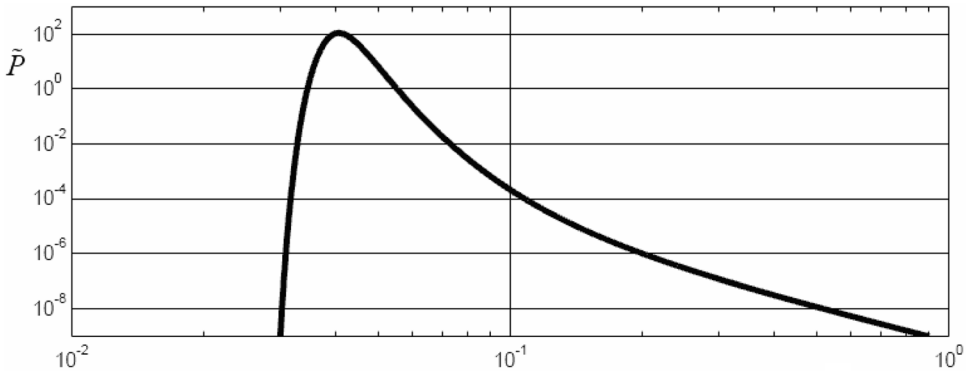

Figure 1. The function $\tilde{\mathbf{P}}(\tilde{\omega})$ (equation (58)).

[67] The structure of $\tilde{P}$ is shown in Figure 1. It rises extremely fast from $\tilde{P} = 5.4 \times 10^{-176}$ at $\tilde{\omega} = 0.024$ to the maximum $\tilde{P} = 108.72$ at $\tilde{\omega} = 0.041$, and then decreases to $\tilde{P} = 3.78 \times 10^{-11}$ at $\tilde{\omega} = 2$.

[68] An anonymous reviewer has mentioned the fact that $\tilde{\omega} = 0.041$, which separates the increasing part of $\tilde{P}$ from the decreasing one, has the same numerical value as $u^*\omega_p/g$, which separates mature wavefields from young wavefields (having their spectral peak frequency denoted by ω_p); see *Babanin and Soloviev* [1998].

[69] The frequency spectrum of the free surface, (42) is written as

$$\tilde{s} = 25\pi\left(\frac{\rho_a}{\rho_w}\right)^2\left(e^{2\tilde{\beta}\tilde{x}} - 1\right)\tilde{P}, \tag{60}$$

where

$$\tilde{\beta} = 0.08\tilde{k}^2, \tag{61a}$$

$$\tilde{x} = gx/u_*^2 \tag{61b}$$

[70] For $\rho_a = 1.2\ kg/m^3$ and $\rho_w = 1025\ kg/m^3$, (60) reduces to

$$\tilde{s} = 1.076 \times 10^{-4}\left\{\exp\left(0.16\tilde{\omega}^4\tilde{x}\right) - 1\right\}\tilde{P} \tag{62}$$

[71] From (57) one can see that the dimensionless form of the limiting spectrum is

$$\tilde{s}_h = \alpha\tilde{\omega}^{-5} \tag{63}$$

[72] For any given $(\tilde{x}, \tilde{\omega})$, the overall spectrum is given by the $\inf(\tilde{s}, \tilde{s}_h)$.

[73] The overall spectra, for a wide range on $\tilde{x}$ are shown in Figure 2, in log-log scale.

[74] The points where $s = s_h$ are at the spectral peak frequency $\tilde{\omega}_p$. The values of the peak frequencies as a function of α and $\tilde{x}$ are given in Table 1.

[75] The variation of $\log \tilde{\omega}_p$ as a function of $\log \tilde{x}$ is shown in Figure 3.From Figure 3, one finds that

$$\tilde{\omega}_p = (3.65 \pm 0.11) \cdot \tilde{x}^{-0.25} \tag{64}$$

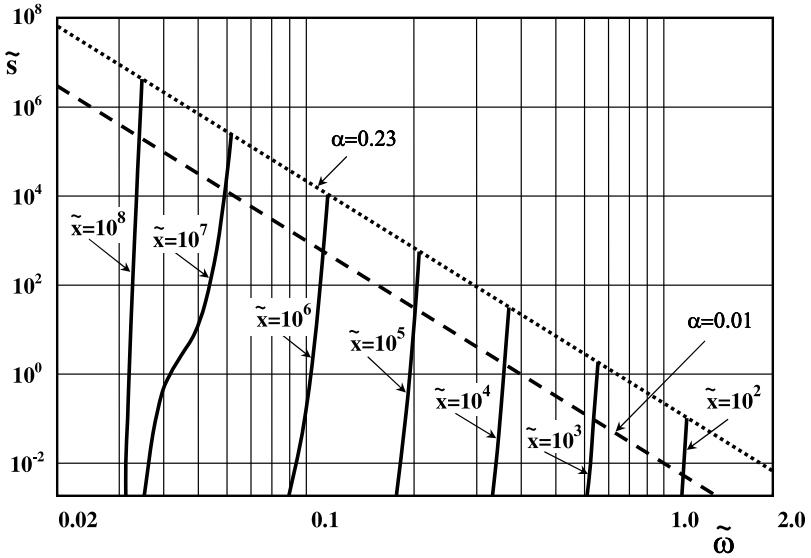

Figure 2. Frequency spectra of the free surface $\tilde{s}(\tilde{\omega})$, for various fetch lengths $\tilde{x}$. Solid curves are $\tilde{s}$ from (62). Dotted and dashed lines are $\tilde{s}_h$ from (63) with α = 0.23 and 0.01, respectively.

Table 1. Values of $\tilde{\omega}_p$ From Figure 2

	$\alpha = 0.01$	$\alpha = 0.23$
$\tilde{x} = 10^2$	1.128	1.162
$\tilde{x} = 10^3$	0.636	0.654
$\tilde{x} = 10^4$	0.359	0.369
$\tilde{x} = 10^5$	0.202	0.207
$\tilde{x} = 10^6$	0.112	0.115
$\tilde{x} = 10^7$	0.060	0.062
$\tilde{x} = 10^8$	0.035	0.035

[76] Thus, within the accuracy of about 3%, we have

$$\tilde{\omega}_p = 3.65\,\tilde{x}^{-0.25} \tag{65}$$

[77] From Figure 2 it is clear that, within a similar level of accuracy, the total dimensionless energy content for any $\tilde{\omega}_p$ is given by

$$\tilde{e} = \alpha \int_{\tilde{\omega}_p}^{\infty} \tilde{\omega}^{-5} d\tilde{\omega} = 0.25\,\alpha\,\tilde{\omega}_p^{-4} \tag{66}$$

[78] Substituting (65) into (66) gives

$$\tilde{e} = 1.4 \times 10^{-3} \alpha \tilde{x} \tag{67}$$

[79] To determine the value of α, we rely on experimental results which are summarized by *Badulin et al.* [2007, Table 2]. We use the averages of experiments 1.1 to 1.4 which Badulin et al. call the "cleanest."

[80] According to these experimental results, the exponents of $\tilde{x}$ in (65) and (67) are (0.27 ± 0.2) and (0.9 ± 0.1), respectively, in agreement with our theoretical finding of 0.25 and one.

[81] It is important to note that *Badulin et al.* [2007] use U_h (the wind velocity at 10 m above the surface) as their scaling velocity; whereas our theory uses the shear velocity u^*. According to Badulin et al.

$$\tilde{\omega}_p = 13.9\,\delta^{1/2}\,\tilde{x}^{-0.27} \tag{68a}$$

where $\delta = u^*/U_h$. Taking a typical fetch $\tilde{x} = 10^5$, enables to rewrite (68a):

$$\tilde{\omega}_p = 17.5\,\delta^{1/2}\,\tilde{x}^{-0.25} \tag{68b}$$

Comparing (68b) with (65) gives $\delta = 0.04$.

[82] For the energy, *Badulin et al.* [2007] have

$$\tilde{e} = 5.2 \times 10^{-7}\,\delta^{-2}\tilde{x}^{0.9} \tag{69a}$$

[83] For a typical fetch of $\tilde{x} = 10^5$, (69a) is rewritten as

$$\tilde{e} = 1.64 \times 10^{-7}\,\delta^{-2}\tilde{x} \tag{69b}$$

[84] Substituting $\delta = 0.04$ into (69b) gives

$$\tilde{e} = 1.03 \times 10^{-4}\,\tilde{x} \tag{69c}$$

[85] Comparing (69c) with (67) gives $\alpha = 0.074$, well below the upper bound of 0.23. The significant wave height is given by

$$\tilde{H}_s = 2\sqrt{2}\,\tilde{e}^{1/2} = 0.029\,\tilde{x}^{1/2} \tag{70}$$

[86] To obtain a measure for the "steepness" ε, we take

$$\varepsilon = \tilde{k}_p\,\tilde{e}^{1/2} = \tilde{\omega}_p^2\,\tilde{e}^{1/2} = 0.13 \tag{71}$$

which turns out to be independent of both, the fetch x, and the shear velocity u^*.

[87] The peak frequency ω_p (65) and the significant wave height H_s (70) in dimensional variables are given by:

$$\omega_p = 3.65\,g^{0.75}\,u_*^{-0.5}\,x^{-0.25} \tag{72}$$

$$H_s = 0.029\,g^{-0.5}\,u_*\,x^{0.5} \tag{73}$$

which are the main results of this note.

[88] The dimensionless spectrum of the waves $\inf(\tilde{s}, \tilde{s}_h)$, as a function of $\tilde{\omega}$, and for $\tilde{x} = 10^4$, is shown in Figure 4, as an example. It is quite clear that nonlinear interactions, which are not included herein, will act to smooth the spectrum at the vicinity of the peak, and to transfer energy to frequencies somewhat lower than $\tilde{\omega}_p = 0.369$.

8. Discussion

8.1. Comparison With the Radiative Transfer Equation

[89] From *Sobey* [1986], the steady one dimensional radiative transfer equation, with a wind input term on its r.h.s., written for $s(x, \omega)$, reads

$$\frac{ds}{dx} = 2\beta s + \frac{4\pi k^5}{\rho_w^2 \omega^4} \int P_3(k\cos\theta, k\sin\theta, \omega)\, d\theta, \tag{74}$$

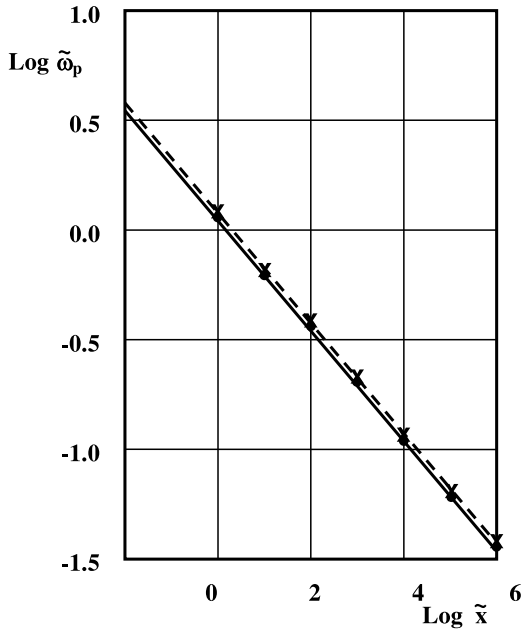

Figure 3. $\tilde{\omega}_p$ versus $\tilde{x}$. Dots are for $\alpha = 0.01$, and crosses for $\alpha = 0.23$. Lines represent the best fit.

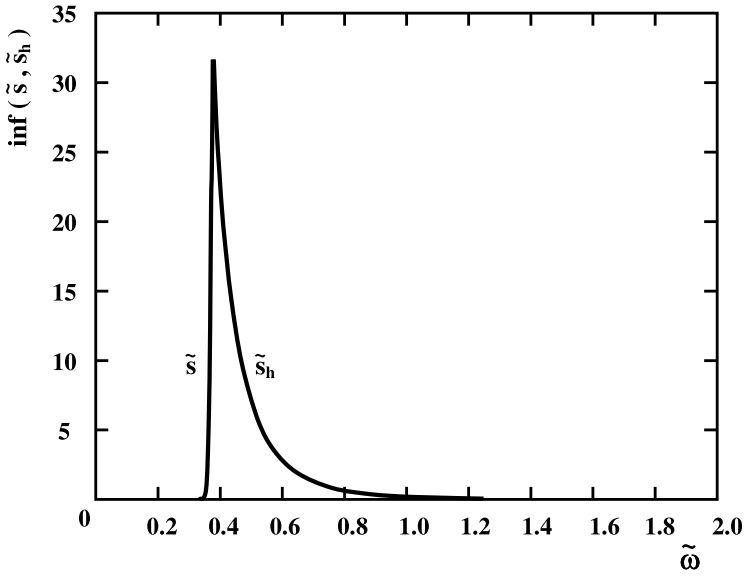

Figure 4. Spectrum of waves for $\tilde{x} = \mathbf{10^4}$.

where P_3, Π is Sobey's notation, is the wave number frequency spectrum of the turbulent atmospheric pressure at the water surface, given in (43). The solution of the O.D.E. (74), for $s\,(0, \omega) = 0$, is

$$s = \frac{2\pi k^5 \left(e^{2\beta x} - 1\right)}{\rho_w^2 \omega^4 \beta} \int P_3(k\cos\theta, k\sin\theta, \omega) d\theta \qquad (75)$$

[90] Comparing (75) to (42) gives

$$P(k, \omega) = k \int P_3(k\cos\theta, k\sin\theta, \omega) d\theta \qquad (76)$$

[91] Given Lysak's result (43), the integral on the r.h.s. of (76) is rather complicated and we have simplified it by taking

$$P(k, \omega) = 2k_e P_3(k, 0, \omega) \qquad (77)$$

where k_e is given by (45a).

[92] The novelty of this note is in the application of *Lysak*'s [2006] theoretical result for P_3 to the wind-wave generation problem. Note that neither *Sobey* [1986], nor anybody else known to us, provide theoretically based expressions for P_3. The state of the art is summarized by *Young* [1999] where references for an empirically, rather crude, estimate for P_3 are cited.

8.2. Comparison With Measurements

[93] *Hwang* [2006] attempts to summarize measured data from various sources in a unified approach. In Figure 5, his results for the total dimensionless spectral energy content $\tilde{e}$ and the dimensionless peak frequency $\tilde{\omega}_p$, as functions of the dimensionless fetch $\tilde{x}$ are plotted together with our calculations.

[94] The dots in Figure 5 are experimental results, the lines represent Hwang's analytical expressions, and the hollow squares and triangles are the new theoretical results, obtained from (65) and (69c). The fit obtained in Figure 5 strengthens our confidence in the relevance of the turbulent pressure spectrum (43) proposed by *Lysak* [2006], for the modeling of the lower part of the marine boundary layer.

8.3. On Other Source Terms of the Radiative Transfer Equation

[95] Following the prevailing convention [see *Sobey*, 1986], the r.h.s. of (74) should include two additional

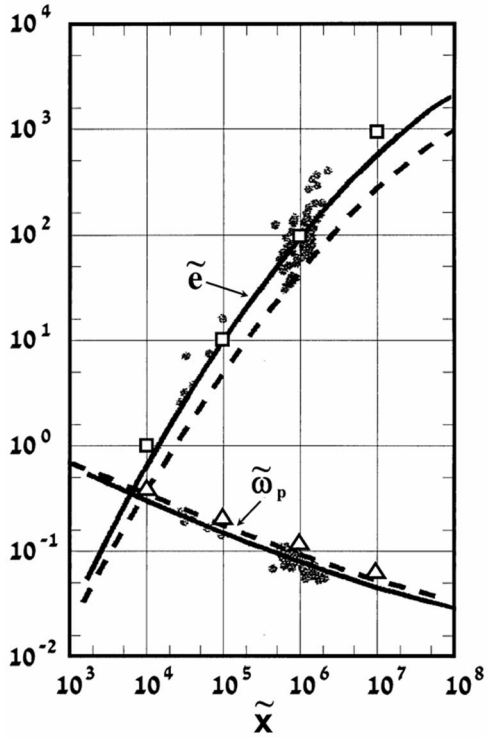

Figure 5. Fetch-limited growth: comparison with available field data.

source terms: a dissipation term, and a term representing the nonlinear interactions among the spectral modes.

[96] The major mechanism for dissipation is due to wave breaking; for which it is extremely difficult to provide a theoretical model in the frequency domain. On the other hand, the mathematical formulation of nonlinear interactions is well established since the early work of *Hasselmann* [1962], see also *Mei et al.* [2005].

[97] In this note, dissipation is taken into account by introducing the concept of the "limiting spectrum" (in analogy to that of the "highest wave"); but the effects of nonlinear interaction are ignored.

[98] An important result of this paper is the fact that the main features of the spectrum (i.e., peak frequency and total energy), were obtained despite the neglect of nonlinear interactions. It seems that the wind input term (43) plays a major role in the generation of waves on all scales (including those at low frequencies), in contrast to the opinion that most of the input is at the higher-frequency part of the spectrum, and that nonlinear interactions are the main "agent" in the energy transfer to low frequencies. Nevertheless, other observed features, such as the overshoot phenomenon, cannot be reproduced without including nonlinear effects in the radiative transfer equation.

[99] **Acknowledgment.** This research was supported by the Israel Science Foundation, grant 1194/07.

References

Babanin, A. V. (2011), *Breaking and Dissipation of Ocean Surface Waves*, 463 pp., Cambridge Univ. Press, Cambridge, U. K., doi:10.1017/CBO9780511736162.

Babanin, A. V., and Y. P. Soloviev (1998), Field investigation of transformation of the wind wave frequency spectrum with fetch and stage of development, *J. Phys. Oceanogr.*, *28*, 563–576, doi:10.1175/1520-0485(1998)028<0563:FIOTOT>2.0.CO;2.

Badulin, S. I., A. V. Babanin, V. E. Zakharov, and D. Resio (2007), Weakly turbulent laws of wind-wave growth, *J. Fluid Mech.*, *591*, 339–378, doi:10.1017/S0022112007008282.

Hasselmann, K. (1962), On the nonlinear energy transfer in a gravity-wave spectrum. Part 1. General theory, *J. Fluid Mech.*, *12*, 481–500, doi:10.1017/S0022112062000373.

Hwang, P. A. (2006), Duration-and fetch-limited growth functions of wind-generated waves parameterized with three different scaling wind velocities, *J. Geophys. Res.*, *111*, C02005, doi:10.1029/2005JC003180.

Lysak, P. D. (2006), Modeling the wall pressure in turbulent pipe flows, *J. Fluid Eng. Trans. ASME*, *128*, 216–222.

Mei, C. C., M. Stiassnie, and D. K. P. Yue (2005), *Theory and Applications of Ocean Surface Waves—Part 2: Nonlinear Aspects*, *Adv. Ser. on Ocean Eng.*, vol. 23, World Sci., Singapore.

Miles, J. W. (1957), On the generation of surface waves by shear flows, *J. Fluid Mech.*, *3*, 185–204, doi:10.1017/S0022112057000567.

Phillips, O. M. (1957), On the generation of waves by turbulent wind, *J. Fluid Mech.*, *2*, 417–445, doi:10.1017/S0022112057000233.

Plant, W. J. (1982), A relationship between wind stress and wave slope, *J. Geophys. Res.*, *87*(C3), 1961–1967, doi:10.1029/JC087iC03p01961.

Sobey, R. J. (1986), Wind-wave prediction, *Annu. Rev. Fluid Mech.*, *18*, 149–172, doi:10.1146/annurev.fl.18.010186.001053.

Stiassnie, M., Y. Agnon, and P. A. E. M. Janssen (2007), Temporal and spatial growth of wind waves, *J. Phys. Oceanogr.*, *37*(1), 106–114, doi:10.1175/JPO2982.1.

Young, I. R. (1999), *Wind Generated Ocean Waves*, 288 pp., Elsevier, New York.

Zakharov, V. E. (2005), Theoretical interpretation of fetch limited wind-driven sea observations, *Nonlinear Processes Geophys.*, *12*, 1011–1020, doi:10.5194/npg-12-1011-2005.

M. Stiassnie, Department of Civil and Environmental Engineering, Technion–Israel Institute of Technology, Haifa 32000, Israel. (miky@tx.technion.ac.il)